Hypoxia in Human Gliomas: Demonstration by PET with Fluorine-18-Fluoromisonidazole

Peter E. Valk, Chester A. Mathis, Michael D. Prados, John C. Gilbert and Thomas F. Budinger

Lawrence Berkeley Laboratory, University of California, Berkeley; University of California School of Medicine, San Francisco, California

Positron emission tomography (PET) with the hypoxic-cell tracer [^{18}F]fluoromisonidazole presents a possible means of noninvasively demonstrating tumor hypoxia. PET studies using this tracer were performed in three patients with malignant glioma, and in all patients the tumor was clearly seen at 5 min postinjection and initial tumor activity exceeded cortical activity. In one patient, there was no tumor retention of [^{18}F] fluoromisonidazole and tumor activity fell while cortical activity increased, with the two tissues reaching equality at 40–50 min. The tumor-to-plasma ratio was 0.71 at 3 hr. The other two patients showed variable tumor retention of [^{18}F]fluoromisonidazole, with tumor-to-plasma ratios of 1.10 and 1.49 at 2 and 3 hr. These results demonstrate the feasibility of using [^{18}F]fluoromisonidazole PET to detect hypoxia in human gliomas in vivo. Clinical trials are needed to determine whether a relationship exists between [^{18}F]fluoromisonidazole uptake and tumor radiation response.

J Nucl Med 1992; 33:2133–2137

It has been known since the 1930s that cells are more sensitive to radiation in the presence of oxygen than in its absence (*1,2*). As a result, tumor hypoxia may have major significance in radiation therapy, as even a small percentage of hypoxic cells within a tumor could limit response to radiation. Hypoxic radioresistance has been demonstrated in many experimental and animal tumors (*3*) but in man hypoxia has been directly demonstrated in only a few tumor types (*4,5*). The occurrence of hypoxia in human tumors has in most cases been inferred from histologic findings and from evidence of hypoxia in animal tumor studies. In vivo demonstration of hypoxia has required tissue measurements with oxygen electrodes and the invasiveness of this technique has limited its application.

Despite the lack of direct evidence of hypoxia in most human tumors, the potential role of hypoxia in cell killing has had a major effect on the direction of radiation therapy research, leading to the evaluation of hyperbaric oxygen therapy (*6*) and the development of chemical radiosensitizers (*7*). Positron emission tomography (PET) with [^{18}F] fluoromisonidazole now presents a possible means of noninvasively demonstrating tumor hypoxia. Fluoromisonidazole is a fluorinated analog of the chemical radiosensitizer misonidazole and distribution studies in tumor and non-tumor tissue have demonstrated labeling specificity for viable hypoxic cells (*8–10*). We performed PET studies with [^{18}F]fluoromisonidazole in three patients with malignant glioma, as a preliminary evaluation of this radiopharmaceutical for the detection of hypoxia in human brain tumors in vivo.

METHODS

Fluorine-18-fluoromisonidazole was synthesized according to the method described by Grierson et al. (*11*). The radiochemical purity of the compound was >97% and the specific activity was determined to be 1000 Ci/mmole at the end of the synthesis.

Imaging was performed with the single-section Donner 280-crystral tomograph. The intrinsic in-plane resolution of this instrument is 8 mm FWHM in the center of the field and axial resolution is 11 mm FWHM (*12*). Three patients were studied, one with highly-anaplastic astrocytoma and two with glioblastoma multiforme. Two intravenous cannulae were inserted, one for injection of radiopharmaceuticals and the other for collection of blood samples. The patients were then placed supine on the tomograph table, which was positioned to obtain transaxial images at the level of the tumor, as determined from x-ray computed tomographic images. An individually-molded thermoplastic head holder was used for head restraint.

Rubidium-82 imaging of the tumor was performed first, to demonstrate the extent of blood-brain barrier (BBB) defect (*13*). Approximately 15 mCi (555 MBq) of ^{82}Rb ($t_{½}$ 76 sec) were injected per image level and data were acquired for 7 min after injection. Tracer elution and injection were performed with an automated ^{82}Sr-^{82}Rb generator-infusion system (*14*). The number of sections imaged was determined by the extent of the tumor. Blood-brain barrier images were obtained by summing the data acquired between 100 and 300 sec postinjection. After the ^{82}Rb study, transmission data were acquired at each anatomic level, using a ^{68}Ge-^{68}Ga source, distributed in a hoop external to the patient (*12*). Typically, 20×10^6 events were collected in 10 min per transverse section.

An anatomic level was selected for dynamic data acquisition

Received Feb. 11, 1992; revision accepted Jul. 21, 1992.

For reprints contact: Peter E. Valk, MD, Northern California PET Imaging Center, 3195 Folsom Blvd., Sacramento, CA 95816.

TABLE 1
Patient Data

Patient (age, sex)	Histological diagnosis	Therapy before PET	PET	Progress after PET result
29, M	Anaplastic astrocytoma	Partial resection 1 mo earlier	+	RT, CRX. Recurrence at 4 mo, resection & CRX; well 1 yr later
49, M	Glioblastoma multiforme	Partial resection 2 mo and 3 mo earlier, RT completed 1 mo earlier	+++	CRX. Rapid progression, died 3 mo later
45, M	Glioblastoma multiforme	Partial resection 1 mo earlier	–	RT, CRX. Recurrence, spinal metastasis & radionecrosis 6 mo later; resection, RT, CRX. Died 1 yr later

RT = radiation therapy and CRX = chemotherapy.

on the basis of CT and ^{82}Rb PET images and approximately 10 mCi (370 MBq) of [^{18}F]fluoromisonidazole were injected intravenously. Dynamic data were acquired for 30 min. Thereafter, the bed was repositioned and data were acquired sequentially for 5 min each from adjacent image sections, until the whole tumor volume had been imaged. This imaging sequence was repeated until the end of the study, 2–3 hr after injection. All ^{82}Rb and ^{18}F emission data were corrected for tissue attenuation using data from the transmission images. Venous blood samples were collected at 1, 2 and 3 hr after [^{18}F]fluoromisonidazole injection for comparison of tissue and plasma radioactivity.

At the end of the study, the blood samples were counted in a well-counter, together with a standard of the injected [^{18}F]fluoromisonidazole dose. The standard was also counted in the tomograph ring and the well-counter data were converted to equivalent PET events per second. Regions of interest (ROIs) were drawn manually in the 5-min images to outline the tumor and the contralateral cerebral cortex. Tissue time-activity curves were generated from the PET data and tumor-to-blood activity ratios were calculated.

RESULTS

In all patients, the ^{82}Rb images showed evidence of a BBB defect at the site of the tumor and the initial [^{18}F] fluoromisonidazole activity at this site exceeded the activity in the normal cortex. The tumors were clearly delineated in [^{18}F]fluoromisonidazole images that were acquired during the first 5 min after injection (Figs. 1A and 2A). The tracer crossed the intact BBB more slowly, so that cortical activity increased gradually, reaching a maximum approximately 40 min after injection and then declining in parallel with blood activity.

In one patient with glioblastoma multiforme, there was no retention of [^{18}F]fluoromisonidazole by the tumor and tumor activity fell after the initial peak, while cortical activity increased (Fig. 1B). Activities in the two tissues reached approximate equality 40–50 min postinjection and remained approximately equal to the end of the study at 172 min. In the other two patients, one with glioblastoma multiforme (Fig. 2B) and the other with highly anaplastic astrocytoma, the tumor showed retention of [^{18}F]fluoromisonidazole and tumor activity exceeded blood and cortical activity at all times (Table 2).

DISCUSSION

Most attempts to increase the radiosensitivity of tumors by administration of chemical radiosensitizers have been unsuccessful (*7*). However, there has been no clinically-applicable means of demonstrating tumor hypoxia and it has not been possible to identify the patients who could potentially benefit from radiosensitizing therapy.

Evidence of a relationship between tumor oxygenation and radiosensitivity in man was reported by Kolstad et al. (*15*) and Gatenby et al. (*4*). Gatenby et al. correlated directly-measured tumor oxygen content with radiation response in 31 patients with metastatic squamous cell cancer of the head and neck. They found that when the hypoxic fraction was more than 26%, no complete responses were achieved; when the hypoxic fraction was less than 26%, the complete response rate was 95%. No other correlations of tumor hypoxia and radiation response have been reported to date to confirm these findings.

Brain tumor hypoxia was demonstrated recently in a study of 16 patients undergoing attempted resection of previously untreated tumors (*16*). Oxygen pressure in the tumor and in surrounding brain was measured at the time of surgery, using an oxygen pressure sensor designed for intravascular use. The mean tumor pO_2 was 15.3 ± 2.3 mmHg, significantly lower than the pO_2 in adjacent normal brain which was 59.8 ± 6.5 mmHg. There was no correlation between intratumoral pO_2 and angiographic or contrast-enhanced CT images of the tumor vasculature. These results showed that hypoxia of sufficient severity to cause hypoxic radiation resistance (*5*) does occur in human brain tumors, so that in vivo demonstration of hypoxia may have significance for patient management.

PET with [^{18}F]fluoromisonidazole may facilitate the study of tumor oxygenation by providing a noninvasive

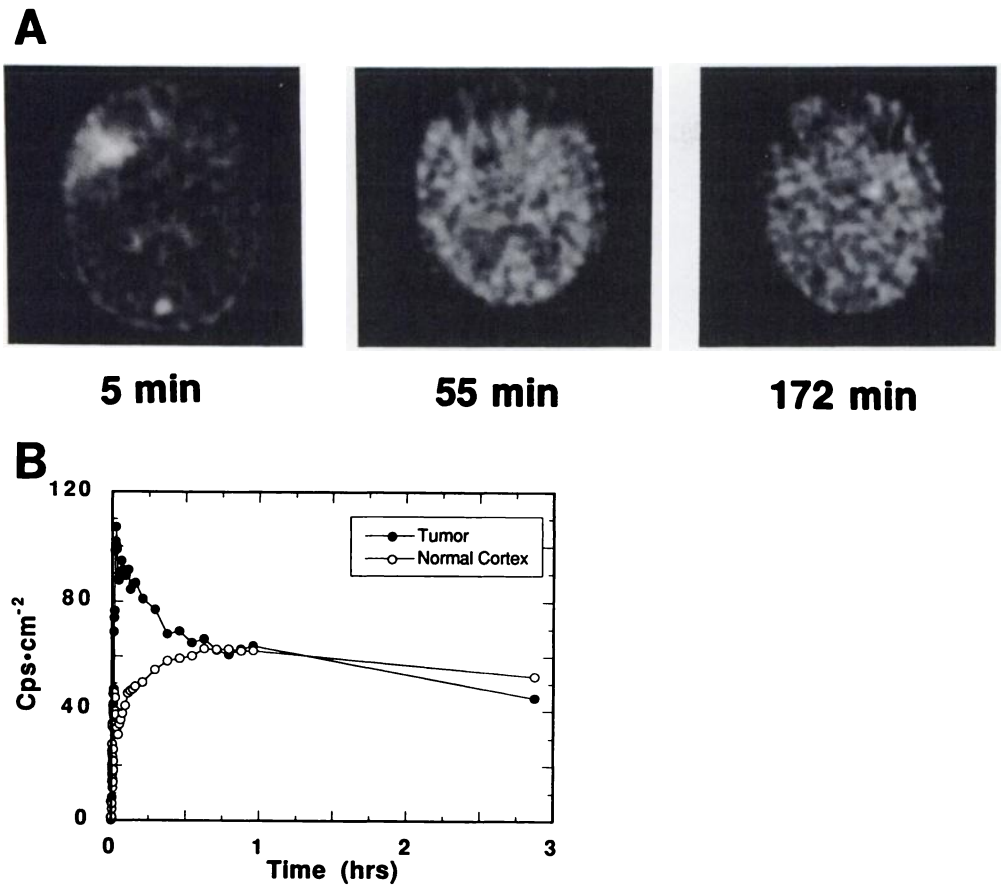

FIGURE 1. Patient 1. (A) PET images and (B) time-activity curves, obtained after IV injection of [^{18}F]fluoromisonidazole. Tumor activity is apparent in the 5-min image. The site of tumor activity corresponds to the site of BBB defect, as shown previously with ^{82}Rb. Thereafter, uptake by normal cortex increases gradually, indicating slower passage of tracer across the intact BBB, and tumor activity falls. Activities in the two tissues reach approximate equality at 40–50 min and remain approximately equal until the end of the study at 172 min. The time-activity curves show no evidence of tumor hypoxia.

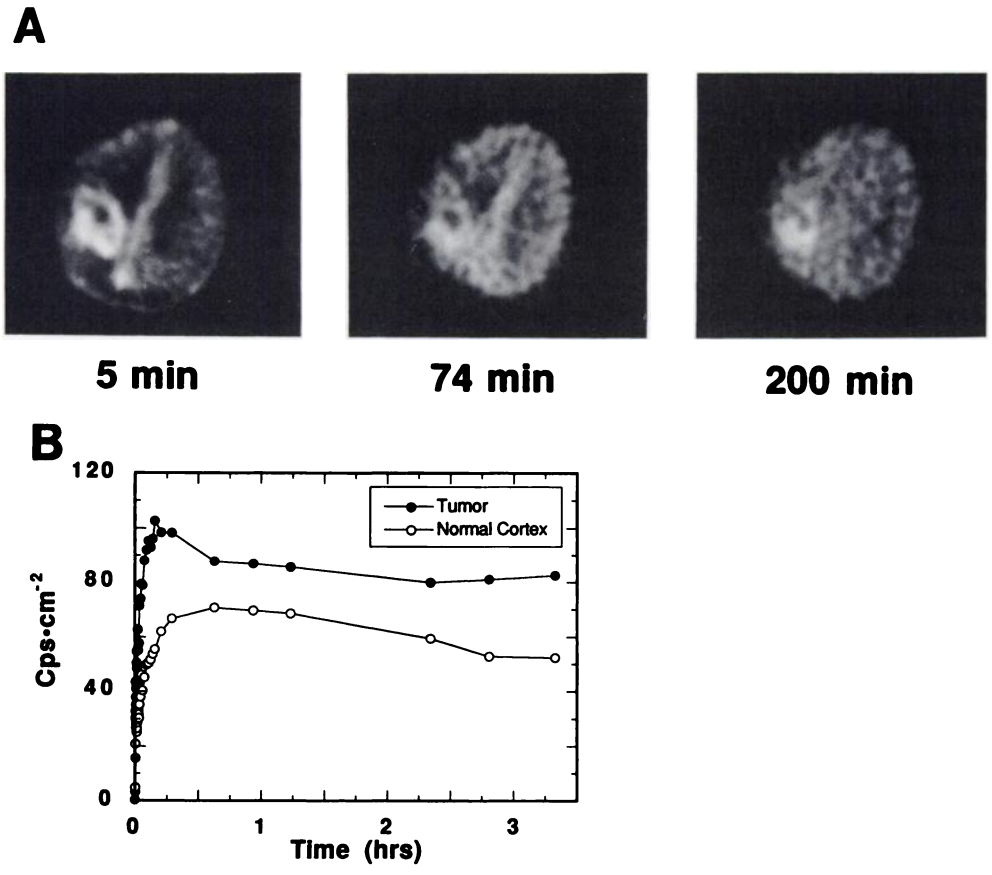

FIGURE 2. Patient 3. (A) PET images and (B) time-activity curves, obtained after intravenous injection of [^{18}F]fluoromisonidazole. Tumor activity is apparent in the 5-min image. The site of tumor activity corresponds to the site of BBB defect, as shown previously with ^{82}Rb. Uptake by normal cortex increases gradually, indicating slower passage of tracer across the intact BBB. There is an initial decrease in tumor activity, possibly reflecting a subpopulation of normoxic cells, but activity within the lesion remains higher than cortical activity at all times. After 40 min, tumor activity approximately parallels cortical activity to 140 min and then increases slightly to the end of the study. Apparent fixation of activity by the tumor is consistent with tumor hypoxia.

TABLE 2
Tumor Uptake Ratios

Patient no.	Time	Tumor/Plasma	Cortex/Plasma
1	1 hr	0.84	0.82
	3 hr	0.71	0.82
2	1 hr	1.14	0.84
	2 hr	1.10	0.87
3	1 hr	1.30	1.04
	2 hr	1.30	0.99
	3 hr	1.49	0.94

means of detecting hypoxic tissue. Fluoromisonidazole is structurally and biologically similar to the nitroimidazole radiosensitizing drug misonidazole (*9*). Misonidazole and fluoromisonidazole both have high electron affinity and are selectively reduced and bound in viable hypoxic cells. In studies with [^{14}C]misonidazole in cell cultures and in mice, it was shown that loss of misonidazole adducts from hypoxic tumor cells occurred with a half-life of 50 hr, while unbound misonidazole cleared from normoxic tissue with a half-life of 0.7 hr (*17*). Synthesis of [^{18}F]fluoromisonidazole was described by Jerabek (*18*) and was further developed by Grierson et al. (*11*). Rasey et al. showed that the distribution of fluoromisonidazole in tumor cells was similar to the distribution of misonidazole, and confirmed the viable hypoxic-cell specificity of the fluorinated analog (*10*). Koh et al. subsequently demonstrated [^{18}F]fluoromisonidazole uptake in human head and neck tumors and showed marked decrease in [^{18}F]fluoromisonidazole binding post-irradiation, indicating that tumor reoxygenation was taking place during therapy (*19,20*).

The effects of oxygen on misonidazole binding and radiation resistance occur at similar concentrations in vitro. The K_m of misonidazole binding inhibition (oxygen concentration at a rate of binding midway between the rates observed in air and in nitrogen) for 12 tumor cultures, including human colon carcinoma, melanoma and breast carcinoma, was shown to range from 0.1%–0.6% (*17*). These values are similar to the range of K_m's for oxygen enhancement of radiation sensitivity, which is approximately 0.3%–0.5% (*21*). Binding inhibition of fluoromisonidazole occurs at similar oxygen concentrations (*10*).

The significance of in vivo [^{18}F]fluoromisonidazole uptake by human tumors must be determined by correlation of PET findings with response to radiation therapy in a statistically significant number of patients. Results obtained with in vitro tumor cultures and experimental animal tumors suggest a complex relationship between [^{18}F]fluoromisonidazole binding and tumor hypoxia. Quantitation of tumor oxygenation by measurement of [^{18}F]fluoromisonidazole uptake has been hampered by the finding of differences in the oxygen-dependence of [^{18}F] fluoromisonidazole binding by different experimental tumor types in vitro (*22–24*). It is not yet known if such differences also occur in human tumors in vivo. Even if such variations do occur, it may be possible to relate [^{18}F] fluoromisonidazole uptake to radiation response for specific tumor types, such as anaplastic astrocytoma or glioblastoma multiforme, and to use the PET measurement of tracer retention as a clinically applicable assessment of tumor oxygenation.

Assessment of tumor hypoxia prior to radiation therapy would provide a rational means of selecting patients for treatment with chemical radiosensitizing drugs. Such selection of patients would permit more accurate evaluation of radiosensitizing drugs, since their use could be limited to patients with hypoxic tumors, who could potentially benefit from the drug. The relationship of [^{18}F]fluoromisonidazole uptake to tumor radiation response in vivo is the only end-point of clinical significance, and this can only be determined by appropriate clinical trials. The preliminary findings reported here indicate that such trials would be warranted.

REFERENCES

1. Mottram JC. Factors of importance in the radiosensitivity of tumors. *Br J Radiol*1936;9:606–614.
2. Powers WE, Tolmach LJ. A multi-component x-ray survival curve for mouse lymphosarcoma cells irradiated in vivo. *Nature* 1963;197:710–711.
3. Moulder JE, Rockwell S. Hypoxic fractions of solid tumors: experimental techniques, methods of analysis and a survey of existing data. *Int J Radiat Oncol Biol Phys* 1984;10:695–712.
4. Gatenby RA, Kessler HB, Rosenblum SJ, et al. Oxygen distribution in squamous cell carcinoma metastases and its relationship to outcome of radiation therapy. *Int J Radiat Oncol Biol Phys* 1988;14:831–838.
5. Cater DB, Silver LA. Quantitative measurements of oxygen tension in normal tissues and in the tumors of patients before and after radiotherapy. *Acta Radiol* 1960;53:233–256.
6. Dische S. What have we learned from hyperbaric oxygen? *Radiother Oncol* 1991;20, (suppl 1):71–74.
7. Dische S. A review of hypoxic-cell radiosensitization. *Int J Radiat Oncol Biol Phys* 1991;20:147–152.
8. Martin GV, Caldwell JH, Rasey JS, Grunbaum Z, Cerqueira M, Krohn KA. Enhanced binding of the hypoxic cell marker [^{18}F]fluoromisonidazole in ischemic myocardium. *J Nucl Med* 1989;30:194–201.
9. Rasey JS, Grunbaum Z, Magee S, et al. Characterization of radiolabeled fluoromisonidazole as a probe for hypoxic cells. *Radiat Res* 1987;111: 292–304.
10. Rasey JS, Koh W, Grierson JR, Grunbaum Z, Krohn KA. Radiolabeled fluoromisonidazole as an imaging agent for tumor hypoxia. *Int J Radiat Oncol Biol Phys* 1989;17:985–991.
11. Grierson JR, Link JM, Mathis CA, Rasey JS, Krohn KA. A radiosynthesis of fluorine-18 fluoromisonidazole. *J Nucl Med* 1989;30:343–350.
12. Derenzo SE, Budinger TF, Huesman RH, et al. Imaging properties of a positron tomograph with 280 BGO crystals. *IEEE Trans Nucl Sci* 1981; NS-28(1):81–89.
13. Yen C-K, Budinger TF. Evaluation of blood-brain permeability changes in Rhesus monkeys using Rb-82 and positron emission tomography. *J Comput Assist Tomogr* 1981;5:792–799.
14. Yano Y, J. L. C, Budinger TF. A precision flow-controlled Rb-82 generator for constant-infusion studies of the heart and brain. *J Nucl Med* 1981;22: 1006–1010.
15. Kolstad P. Intercapillary distance, oxygen tension and local recurrence in cervix cancer. *Scand J Clin Lab Invest* 1968;106 (suppl): 145–166.
16. Kayama T, Yoshimoto T, Fujimoto S, Sakurai Y. Intratumoral oxygen pressure in malignant brain tumors. *J Neurosurg* 1991;74:55–59.
17. Franko AJ. Misonidazole and other hypoxia markers: Metabolism and applications. *Int J Radiation Oncology Biol Phys* 1986;12:1195–1202.
18. Jerabek PA, Patrick TB, Kilbourn MR, Dischino DD, Welch MJ. Synthesis and biodistribution of F-18-labeled fluoronitroimidazoles: potential markers of hypoxic tissue. *Appl Radiat Isot* 1986;37:599–605.

19. Koh WJ, Rasey JS, Grierson JR, et al. Hypoxia imaging of tumors using [F-18]fluoromisonidazole. *J Nucl Med* 1989;30:789.
20. Koh WJ, Rasey JS, Evans ML, et al. Imaging human tumor hypoxia using [F-18]fluoromisonidazole. *J Nucl Med* 1991;32:955.
21. Koch CJ, Stobbe CC, Bump EA. The effect on the Km for radiosensitization at 0° of thiol depletion by diethylmaleate pretreatment: quantitative differences found using the radiation sensitizing agent misonidazole or oxygen. *Radiat Res* 1984;98:141–153.
22. Chapman JD. The cellular basis of radiotherapeutic response. *Radiat Phys Chem* 1984;24:283–291.
23. Franko AJ, Koch CJ, Garrecht BM, Sharplin J, Hughes D. Oxygen dependence of binding of misonidazole to rodent and human tumors in vitro. *Cancer Res* 1987;47:5367–5376.
24. Hirst DG, Hazelhurst JL, Brown JM. Changes in misonidazole binding with hypoxic fraction in mouse tumors. *Int J Radiat Oncol Biol Phys* 1985; 11:1349–1355.

(continued from page 2123)

SELF-STUDY TEST
Pulmonary Medicine
ANSWERS

loaded with two to three times as much activity as used for a conventional preperfusion study. Eventually, breathing from such a nebulizer will allow the aerosol-associated activity in the lungs to exceed that of the ^{99m}Tc particles by a factor of 4 to 5. If a "mismatch" is present, images acquired at this time will show definite entry of aerosol activity into the region of a previously defined perfusion defect (i.e., the perfusion defect will "disappear" as its region becomes filled with inhaled aerosol activity).

References

1. Alderson PO, Martin EC. Pulmonary embolism: diagnosis with multiple imaging modalities. *Radiology* 1987;164:297–312.
2. Agnew JE. Aerosol contributions to the investigation of lung structure and ventilatory function. In: Clarke SW, Pavia D, eds. *Aerosols and the Lung: Clinical and Experimental Aspects*. London: Butterworths, 1984:92–126

ITEMS 6–10: Accelerated Pulmonary Clearance of ^{99m}Tc DTPA Aerosol

ANSWERS: 6, T; 7, T; 8, T; 9, T; 10, T

The pulmonary clearance of ^{99m}Tc DTPA aerosol is accelerated in the presence of any condition that disrupts the alveolar–capillary membrane and increases its permeability. Several studies have demonstrated that this occurs during active cigarette smoking. The underlying changes that occur in the alveolar–capillary membrane in the presence of cigarette smoke are unknown, but some investigators have hypothesized that the changes are related to disruption of the surfactant coating that lines the alveoli and that would normally impede radioaerosol clearance. The adult respiratory distress syndrome, as well as the analogous pediatric condition, hyaline membrane disease, result in disruption of both the alveolar epithelial and endothelial surfaces. In the initial stages of the disease, epithelial disruption occurs without associated leakage of proteins and other blood compartment fluids through the endothelial membrane. The clearance of soluble radioaerosols should be increased at this early stage of the disease when radiographic studies still are frequently normal.

Idiopathic pulmonary fibrosis also is known to be associated with an increased clearance rate of soluble radioaerosols. This may seem paradoxical, because the tissues between the alveolar and vascular linings should be thickened and more difficult to traverse in this disorder. This has led to speculation that radioaerosol clearance occurs, at least in part, through pores between the alveoli and the interstitium surrounding the pulmonary capillaries. Advocates of the pore theory suggest that in the presence of fibrosis the "pores" are held open by the fibrotic interstitial tissues, thus, allowing rapid egress of the radioaerosols. It appears, however, that the accelerated clearance occuring during the active stage of disorders that lead to fibrosis is on the basis of inflammatory disruption of the alveolar–capillary membranes. Residual increases in aerosol clearance probably are the result of irreversible structural damage to the epithelial basement membrane and adjacent tissues.

Technetium-99m DTPA aerosol clearance also appears to be accelerated in regions of pulmonary embolism. Because pulmonary perfusion is markedly reduced or absent in such areas, this may seem surprising. However, bronchial vessels establish collateral blood flow to these areas within hours in humans, and this flow seems capable of supporting clearance of DTPA. Clearance of this tracer is largely dependent on epithelial permeability and is only minimally flow-dependent. Thus, even the lower amounts of blood flow through bronchial collaterals are sufficient to allow clearance to continue. Structural damage to the alveolar–capillary membrane distal to an embolus and, possibly, the additional loss of surfactant provide an excellent basis for increased ^{99m}Tc DTPA clearance. It is important to note, however, that the reported increases in DTPA clearance rates in regions of pulmonary embolism have only been about twice normal, and that sufficient aerosol activity has been present at the time of imaging to allow mismatches to be recognized clearly. The only patients reported to date underwent quantitative aerosol clearance studies 24 hr after an initial ventilation–perfusion study had revealed the regions of mismatch. Whether or not similar changes in aerosol clearance rates occur earlier in the course of pulmonary embolism is unknown.

References

1. Buxton-Thomas M, Higenbottam T, Barber R, Wraight P. Clearance of inhaled ^{99m}Tc DTPA from regions of the lung recently affected by pulmonary embolus. *Bull Eur Physiopathol Respir* 1986;22:55–60.
2. Coates G, O'Brodovich H. Measurement of pulmonary epithelial permeability with ^{99m}Tc-DTPA aerosol. *Semin Nucl Med* 1986;16:275–284.
3. Jefferies AL, Coates G, O'Brodovich H. Pulmonary epithelial permeability in hyaline-membrane disease. *N Engl J Med* 1984;311:1075–1080.
4. Newhouse MI, Jordana M, Dolovich M. Evaluation of lung epithelial permeability. *Eur J Nucl Med* 1987;13:S58–S62.

ITEMS 11–15: Pulmonary Accumulation of Amines

ANSWERS: 11, F; 12, T; 13, T; 14, F; 15, F

The pulmonary accumulation of radioiodinated HIPDM, like the pulmonary accumulation of other radiolabeled amines, is saturable. When low to moderate levels of unlabeled amine are present, there is relatively little effect on the pulmonary accumulation of HIPDM. When relatively large amounts are added, however, the ability of the lungs to accumulate HIPDM is inhibited significantly. This suggests that there are a finite number of binding sites for HIPDM in the lungs. Even more effective inhibition of HIPDM accumulation can be obtained by simultaneous administration of other amines, such as chlorpromazine or propranolol. The pulmonary accumulation of HIPDM is diminished significantly when modest amounts of either of these amines are present. This indicates that these amines and HIPDM compete for the same binding sites.

Pulmonary accumulation of HIPDM is not inhibited by ouabain, a drug known to inhibit energy-dependent processes. Thus, HIPDM accumulation in the lung does not seem to require active transport as provided by the sodium–potassium ATPase system. The pulmonary accumulation of propranolol and other amines has been characterized as a physicochemical uptake in a membrane-related system that is saturable. A similar mechanism probably is operating in the pulmonary accumulation of HIPDM and iodoamphetamines.

References

1. Slosman DO, Brill AB, Polla BS, Alderson PO. Evaluation of [iodine-125]N,N,N′-trimethyl-N′-2-[2-hydroxy-3-methyl-5-iodobenzyl]-1,-3-propanediamine lung uptake using an isolated-perfused lung model. *J Nucl Med* 1987;28:203–208.
2. Touya JJ, Rahimian J, Grubbs DE, Corbus HF, Bennett LR. A noninvasive procedure for in vivo assay of a lung amine endothelial receptor. *J Nucl Med* 1985; 26:1302–1307.

For further in-depth information, refer to the syllabus pages in Nuclear Medicine Self-Study I.